



**HAL**  
open science

## Three-Dimensional Distribution of UBF and Nopp140 in Relationship to Ribosomal DNA Transcription During Mouse Preimplantation Development

Maïmouna Coura Koné, Renaud R. Fleurot, Martine M. Chebrou, Pascale Debey, Nathalie Beaujean, Amélie Bonnet-Garnier

### ► To cite this version:

Maïmouna Coura Koné, Renaud R. Fleurot, Martine M. Chebrou, Pascale Debey, Nathalie Beaujean, et al.. Three-Dimensional Distribution of UBF and Nopp140 in Relationship to Ribosomal DNA Transcription During Mouse Preimplantation Development. *Biology of Reproduction*, 2016, 94 (4), pp.95. 10.1095/biolreprod.115.136366 . hal-02365191

**HAL Id: hal-02365191**

**<https://hal.science/hal-02365191>**

Submitted on 26 May 2020

**HAL** is a multi-disciplinary open access archive for the deposit and dissemination of scientific research documents, whether they are published or not. The documents may come from teaching and research institutions in France or abroad, or from public or private research centers.

L'archive ouverte pluridisciplinaire **HAL**, est destinée au dépôt et à la diffusion de documents scientifiques de niveau recherche, publiés ou non, émanant des établissements d'enseignement et de recherche français ou étrangers, des laboratoires publics ou privés.

**Title: 3D distribution of UBF & Nopp140 in relationship to rDNA transcription during mouse preimplantation development**

**Running Title:** UBF & Nopp140 in mouse early embryos

5 **Summary sentence:** Dynamic redistribution of UBF & Nopp140 occurs in preimplantation embryos underlying nucleogenesis and rDNA transcriptional activity

**Keywords:** nucleolus, NPB, nucleolar proteins, embryo, oocyte, Fluorescence microscopy, RNA FISH, proximity ligation assay, CX-5461, RNA polymerase I

10 **Maimouna Coura Koné<sup>1</sup>, Renaud Fleurot<sup>1</sup>, Martine Chebrou<sup>1</sup>, Pascale Debey<sup>2</sup>, Nathalie Beaujean<sup>1\*</sup>, and Amélie Bonnet-Garnier<sup>1\*</sup>**

1) UMR BDR, INRA, ENVA, Université Paris Saclay, 78350, Jouy en Josas, France

2) Sorbonne-Universités, MNHN, CNRS, INSERM, Structure et instabilité des génomes, 57 rue Cuvier, 75005 Paris Cedex

15 **Grant Support:** The present work was supported by the REVIVE LabEX program from the ANR. M.C. Koné PhD thesis is funded by the Government of Côte d'Ivoire.

**Correspondence:**

Nathalie Beaujean INSERM U1208, INRA USC1361, Stem Cell and Brain Research Institute, Department of Pluripotent stem cells in Mammals, 18 avenue Doyen Lépine, 69675 Bron, France ; nathalie.beaujean@inserm.fr

20 **Additional footnotes.**

\* These senior authors contributed equally to the supervision of this work

## **Abstract**

The nucleolus is a dynamic nuclear compartment that is mostly involved in ribosome subunit biogenesis; however, it may also play a role in many other biological processes, such as the stress response and the cell cycle. Mainly using electron microscopy, several studies have tried to decipher how active nucleoli are set up during early development in mice. In this study, we analyzed nucleologenesis during mouse early embryonic development using 3D-immunofluorescent detection of UBF and Nopp140, two proteins associated with different nucleolar compartments. UBF is a transcription factor that helps maintain the euchromatic state of ribosomal genes; Nopp140 is a phosphoprotein that has been implicated in pre-rRNA processing.

First, using detailed image analyses and the in situ proximity ligation assay (PLA) technique, we demonstrate that UBF and Nopp140 dynamic redistribution between the 2-cell and blastocyst stages (time of implantation) is correlated with morphological and structural modifications that occur in embryonic nucleolar compartments. Our results also support the hypothesis that nucleoli develop at the periphery of NPBs. Finally, we show that the RNA polymerase I inhibitor CX-5461 i) disrupts transcriptional activity, ii) alters preimplantation development and iii) leads to a complete reorganization of UBF and Nopp140 distribution. Altogether, our results underscore that highly dynamic changes are occurring in the nucleoli of embryos and confirm a close link between ribosomal gene transcription and nucleologenesis during the early stages of development.

## INTRODUCTION

The embryonic preimplantation period is when the biological processes that shape long-term development occur. During this period (from fertilization to implantation), mRNA, ribosomes, and proteins of maternal origin ensure the development of the embryo until its own genome is activated, a process known as embryonic genome activation [1–3]. From this time-point, embryonic development will rely on the translation of newly synthesized embryonic mRNA and on the de novo production of ribosomes, which requires the presence of a functional nucleolus.

The nucleolus is a dynamic nuclear compartment that is involved in many biological functions, among which ribosome biogenesis is the most important and best known (for reviews of the relevant literature, see [4,5]). In somatic cells, the nucleolus consists of three following functional compartments that can be clearly distinguished using electron microscopy: the fibrillar centers (FCs), the dense fibrillar component (DFC) that surrounds the FCs, and the granular center (GC) that contains fibrillar structures (for selected reviews, see [6–8]). The structure of the nucleolus is closely linked to its function. Each subcompartment is associated with a specific step in ribosome synthesis (for reviews, see [6,8,9]). Ribosomal genes (rDNA) are located in the FC and are transcribed into single, large rRNA precursors (pre-rRNA) at the junction between the FC and the DFC. Correspondingly, transcriptional machinery components such RNA polymerase I (RNA pol I), the upstream binding factor (UBF), and TATA box-binding protein-associated factor RNA polymerase I subunit B (TIF-1B) are found both at the FC/DFC border and in the DFC. Large pre-rRNA is then processed to generate three ribosomal RNAs: 28S, 18S, and 5.8S. Early processing is mainly performed in the DFC, which contains several proteins such as fibrillarin and Nopp140. These proteins, together with small nucleolar RNA (snoRNA), form RNA-protein

65 complexes called ribonucleoproteins (RNPs) [10]. Later processing and the assembly of the pre-40S and pre-60S ribosomal subunits starts in the GC, where nucleolar proteins such as B23/nucleophosmin1 are present.

This typical nucleolar organization is absent at the beginning of mouse embryonic development. After fertilization, specific structures called Nucleolar Precursor Bodies (NPBs) appear in the  
70 male and female pronuclei as compact fibrillar masses that can be visualized using electron microscopy. At the late 2-cell stage NPBs get involved in the onset of rDNA transcription [11–14]. Indeed, the transcriptional machinery, including RNA pol I and the processing components, are recruited to the cortical region of the NPBs [15–17]. Ribosomal transcription starts at around 45 hphCG (hours post human chorionic gonadotrophin injection; [17]) and gradually increases  
75 until the blastocyst stage [18]. However, during these early stages of embryonic development, NPBs are not equivalent to the nucleoli of somatic cells, and several research teams have tried to disentangle the relationship between the establishment of somatic-like nucleoli (referred to as nucleogenesis) and the recovery of rDNA transcriptional activity.

Indeed, electron microscopy studies have shown that reticulated zones arise at the periphery of  
80 NPBs: the nucleolar compartments (FC, DFC, and GC) appear gradually and form a reticulated structure, while the compact mass disappears progressively over the course of development [13,15,19,20]. In addition, the distributions of some nucleolar proteins have been studied using immunofluorescence microscopy, either from the 1-cell to the 8-cell stage (UBF and Nopp140) or from 1-cell to the blastocyst stage (fibrillarin, B23/nucleophosmin 1 and C23/nucleolin). These  
85 studies suggest that the presence of nucleolar proteins in the cortical region of the NPBs is linked to the appearance of fibrillar and granular structures [15,17,21–24]. However, data fully describing the events that occur between the 8-cell and the blastocyst stage are scarce [25].

In this study, we focused on UBF and Nopp140, two nucleolar proteins that are associated with the FC and DFC compartments of the nucleolus [26,27]. UBF is a transcription factor belonging to the high-mobility group box (HMG-box) class of proteins that activate the transcription of ribosomal genes [28,29]. UBF acts at both the structural and molecular level to promote rDNA transcription. It binds with the upstream control element and with core components of the rDNA promoter. A specific interaction between UBF and TIF-IB is required to recruit RNA pol I and form the preinitiation complex at the transcription start site (for reviews, see [30–32]). UBF has also been found across rDNA repeats and probably maintains ribosomal genes in an open-chromatin state (for a review, see [33]).

Nopp140 is a highly phosphorylated protein that was first identified in rats [34,35]; it shuttles between the nucleolus and the Cajal (coiled) bodies [23,27,36], where it interacts with coilin [36,37]. It has been suggested that Nopp140 is a chaperone that interacts with both classes of snoRNPs, transporting them to the nucleolus [38,39]. Nopp140 is phosphorylated by casein kinase II [40] and interacts with RNA pol I [41].

We therefore decided to analyze the distributions and interactions of these two proteins in mouse preimplantation embryos using immunofluorescent staining. Our analyses spanned the onset of rDNA synthesis during the late 2-cell stage through the blastocyst stage. The aim of these experiments was to reveal the morphological and structural changes that occur during nucleologensis. To further explore the relationship between nucleologensis and rDNA transcription, we also disrupted ribosome biogenesis in the embryos utilizing a novel RNA pol I inhibitor, CX-5461, which was developed for use in cancer therapy [42–44].

## Materials and Methods

### Ethics

As stated by the European Convention on Animal Experimentation and the Society for the Study of Reproduction, all experiments were performed according to the International Guiding Principles for Biomedical Research Involving Animals. NB and ABG have the authorization to work with laboratory animals from the departmental veterinary regulatory service (license N° 78–95 and A78-184) and from the local ethics committee (N° 12/123 - Comethea Jouy-en-Josas/AgroParisTech).

### 120 Harvesting of oocytes & embryos

To obtain oocytes, ovaries were collected from adult (6- to 8-week-old) C57Bl6/CBA F1 female mice and placed in M2 medium (Sigma-Aldrich) supplemented with dibutyryl cyclic AMP (dbcAMP, 100 mg/ml, Sigma-Aldrich) to prevent the spontaneous resumption of meiosis. Oocyte-cumulus complexes were collected by randomly puncturing the ovary with a fine needle. Any follicular cells surrounding the oocytes were mechanically removed by gentle pipetting using a mouth-controlled glass pipette. The oocytes were then transferred into droplets of M2 supplemented with dbcAMP under mineral oil (Sigma-Aldrich) and fixed as described below.

To obtain embryos, adult C57Bl6/CBA F1 female mice were superovulated by intraperitoneally injecting 5 IU of pregnant mare serum gonadotropin (PMSG); a second injection, of 5 IU human chorionic gonadotropin (hCG), followed 48 hours later. The mice were sacrificed, and the 1-cell-stage embryos (23-24 hphCG) were taken directly from the ampullae and placed in M2 medium with 200 µg/ml hyaluronidase (Sigma-Aldrich). The harvested embryos were then cultured in vitro in microdroplets of M16 medium (Sigma-Aldrich) under mineral oil at 37°C in a 5% CO<sub>2</sub>

atmosphere until the following stages: late 2-cell (48 hphCG), early 4-cell (52hphCG), late 4-cell  
135 (58hphCG), early 8-cell (65hphCG), late 8-cell (72hphCG), early 16-cell (75hphCG), late 16-cell  
(81hphCG), morula (93hphCG), late morula (99hphCG), and blastocyst (102hphCG).

### **CX-5461 treatment**

Embryos collected at the 1-cell stage (24hphCG) as described above were cultured at 37°C and in  
140 a 5% CO<sub>2</sub> atmosphere in M16 medium containing 80nM to 1µM of CX-5461 (Adooq) that  
specifically inhibits RNA polymerase I. CX-5461 was prepared as described by Drygin et al.  
[42]. The embryos were transferred to new droplets of M16 + CX-5461 every 24 hours to ensure  
optimal action of the drug.

### **145 Immunofluorescent staining of UBF and Nopp140**

Oocytes and embryos were fixed by placing them in 4% paraformaldehyde (PFA, EMS) in PBS  
for 10 min at room temperature. The zona pellucida were removed under a stereomicroscope  
using 0.1N HCl (Prolabo); the process usually took only a few seconds and occurred at room  
temperature. The oocytes and embryos were then permeabilized for 30 min at room temperature  
150 using 0.5% Triton X100 in 0.2% BSA-PBS (Sigma-Aldrich). Then, the oocytes and embryos  
were incubated in 2% BSA-PBS for 1 hour (to block unspecific binding sites) and processed for  
in toto single or double immunolabeling. The following primary antibodies diluted in 2% BSA-  
PBS were used: an anti-UBF mouse polyclonal antibody (1/100; H00007343-M01; Novus  
Biologicals), an anti-Nopp140 rabbit polyclonal antibody (1/150; RF12 serum; a gift from U.  
155 Thomas Meier, Department of Anatomy and Structural Biology, New York, USA. The embryos  
were then incubated either with anti-UBF and anti-Nopp140 antibodies overnight at 4°C. After



being washed three times with 0.2% BSA-PBS, the embryos were blocked with 2% BSA-PBS for 30 min and incubated for 1 hour at room temperature with anti-mouse or anti-rabbit Cy3- or Cy5-conjugated secondary antibodies (Jackson ImmunoResearch Laboratories Inc., USA), which were diluted (1/200) in 2% BSA-PBS. DNA counterstaining was performed for 15 min at 37°C using 5µM YO-PRO (Invitrogen) in PBS. The embryos were washed using PBS and gently mounted on slides using a large amount of Citifluor antifading agent (AF1 BioValley) to preserve the 3D structure of the nuclei.

#### 165 **Immuno-RNA FISH**

Oocytes and embryos were briefly transferred in four successive solutions at 37°C: first M2 medium, secondly Tyrode's acidic solution (Sigma-Aldrich) , then M2 medium with 10mM PMSF and finally 0.5% PVP-PBS with 10mM phenylmethanesulfonyl fluoride (PMSF; Fluka) . Thereafter we performed a fixation/permeabilization in a solution containing 4% PFA; 0.5% Triton X100; 10mM PMSF; 0.5% PVP; 1µL/mL RNase Inhibitor (RNasin - Promega) in PBS 15 min at 37°C. From this step onwards, all solutions contained RNasin at 1µL/mL. After a rinse in 0.5%PVP-PBS, oocytes and embryos were permeabilized 30 min with 0.5% Triton X100 in 0.5% PVP-PBS and further blocked with 2% BSA-PBS for 1 hour (all these steps were performed at room temperature). In toto double immunolabeling was then performed with anti-UBF and anti-Nopp140 antibodies overnight as described above. After incubation with the secondary antibodies, oocytes and embryos were rinsed in 0.5%PVP-PBS and post-fixed in 2% PFA/0.5% PVP-PBS for 10 min at room temperature. Oocytes and embryos were then permeabilized 45 min with 0.5% Triton X100 in 0.5% PVP-PBS at 37°C, washed briefly and transferred for 30min at 50°C in the pre-hybridization mix containing 50% Formamide (Sigma-Aldrich); 0.5µg/µL tRNA

180 (Sigma-Aldrich); 1X hybridization buffer (2X hybridization buffer was prepared beforehand with  
20% dextran sulfate, 4X SSC; 1mM EDTA, 40mg/mL BSA, 2mg/mL PVP, 0.1% Triton X100,  
diluted in pure grade water). Meanwhile the mix containing the specific oligonucleotide probe  
was denatured 10 min at 85°C and immediately transferred on ice. Oocytes and embryos were  
then transferred in this hybridization mix and incubated overnight at 42°C. Oocytes and embryos  
185 were washed 2x10min in 2XSSC; 0.5%PVP; 0.1% Triton X100 (diluted with pure grade water)  
and gently mounted on slides with Vectashield antifading agent (Eurobio/Abcys) containing  
10µg/mL DAPI (Invitrogen). The Alexa-488 conjugated probe used for RNA-FISH was  
purchased at Eurogentec (5'ETS - AGAGAA AAGAGCGGA GGTTCGGGACTCCAA described  
in [45]).

190

### **Duolink assay**

The Duolink II in situ proximity ligation assay (PLA, Olink Bioscience, Uppsala, Sweden) was  
performed largely in accordance with the manufacturer's instructions; some modifications were  
necessary to adapt the assay to our biological material (1-cell to 16-cell mouse embryos). All  
195 steps were performed in a preheated, humidified chamber. Embryos were fixed for 10 min at  
room temperature using 4% PFA and 1mM PMSF in PBS. After the removal of the zona  
pellucida using 0.1N HCl (as described above), the embryos were transferred to a 0.5%  
polyvinylpyrrolidone-PBS solution (PVP-PBS; Sigma-Aldrich). The embryos were then  
permeabilized for 30 min at room temperature using 0.5% Triton X100 in 0.5% PVP-PBS and  
200 incubated in Olink blocking solution for 30 min at 37°C. In toto double immunolabeling occurred  
overnight at 4°C using anti-UBF mouse polyclonal antibodies and anti-Nopp140 rabbit  
polyclonal antibodies (as described above) in Olink antibody diluent. After being washed twice in

0.5% PVP-PBS for 20 min at room temperature, the embryos were incubated with Olink Plus and Minus PLA probes (0.5X) for 2 hours at 37°C. After two washes (10 min each) in 0.5% PVP-PBS, the embryos were incubated for 1h30 at 37°C in the ligation solution with the ligase (cf. manufacturer's instructions). After two washes (10 min each) in 0.5% PVP-PBS, amplification was performed by incubating the embryos for 2 hours at 37°C in the amplification solution with the polymerase (cf. manufacturer's instructions). After the embryos were washed in 0.5% PVP-PBS, the DNA counterstaining and embryo mounting was performed as described above, except that 10µg/mL DAPI was used.

### **BrUTP microinjection and immunodetection**

To test the efficiency of the CX-5461 treatment, transcription was assessed as previously described [17], at 49 or 52 hphCG. In short, before the microinjection, the embryos were incubated for 30 min at 37°C and in a 5% CO<sub>2</sub> atmosphere in M16 droplets containing 10µg/ml alpha-amanitin ± 1µM CX-5461. Then, the embryos were microinjected with 40 µM BrUTP (Sigma-Aldrich) and 50 µg/ml alpha-amanitin ± 1µM CX-5461. During and after microinjection, the embryos were placed in M2 medium containing 10µg/ml alpha-amanitin ± 1µM CX-5461. Thirty minutes after the microinjection, the embryos were fixed overnight at 4°C in 4%. Embryos were then washed for 30 min with PBS, and permeabilized for 30 min at room temperature using 0.5% Triton X100. After blocking in 2% BSA-PBS, embryos were incubated for 1 hour at 37°C with an anti-BrdU mouse polyclonal coupled with DyLight 488 (1/50; NB500; Novus Biologicals) that recognizes BrUTP [46]. DNA counterstaining was performed with 5µg/mL DAPI (Invitrogen) in PBS for 15 min at 37°C. Finally, the embryos were washed using PBS and mounted on slides as described above.

### **Fluorescence microscopy and image analysis**

The embryos were viewed using either an inverted ZEISS AxioObserver Z1 microscope  
230 (equipped with an ApoTome slider, a Colibri light source, and an Axiocam MRm camera) or a  
ZEISS LSM 700 confocal laser scanning microscope (MIMA2 Platform, INRA). Observations  
were carried out using a 63X oil-immersion objective (NA: 1.3). Entire embryos were scanned  
using a z-distance of 0.37  $\mu\text{m}$  between optical sections. Fluorescent wavelengths of 405, 488,  
555, and 639 nm were used to excite DAPI, DyLight or Alexa 488, Cy3, and Cy5, respectively.  
235 Images treatment were performed using ZEN software as follows: for each embryo, the  
distribution of UBF and Nopp140 was analyzed, section by section through the entire confocal z-  
stack. As many nuclei as possible were analyzed for each embryo. For each z-section several  
criteria were evaluated such as the number of NPBs, the size and shape of each signal, their  
occurrence and their distribution. These data were then reported on an Excel sheet for statistical  
240 analysis.

### **Statistical analyses**

Statistical analyses were conducted using R (v. 3.1.2). We used the Rcmdr interface to perform  
descriptive statistics and the coin and nparcomp packages to perform nonparametric statistics.

## 245 RESULTS

### **Occurrence of UBF and Nopp140 from the late 2-cell stage to the blastocyst stage**

First, we evaluated the occurrence of UBF and Nopp140 proteins in naturally fertilized preimplantation embryos, from the late 2-cell stage through the blastocyst stage. After the embryos had been stained using classical immunofluorescence procedures, we carefully mounted  
250 them on slides to preserve the 3D structure of the nuclei and to facilitate image analysis, section by section through the entire confocal z-stacks. More than 118 embryos were scanned (approximately 12 for each stage). For the sake of clarity, we use the term NPB when the structures presented a central core that showed no sign of DNA staining.

255 As can be seen in Figure 1, UBF and Nopp140 proteins were observed in the nuclei of embryos of all stages. However, in early-stage embryos, the two proteins were not always associated with NPBs. NPBs either i) displayed both Nopp140 and UBF signals (Nopp140/UBF-NPB); ii) displayed the Nopp140 signal only (Nopp140-NPB); or iii) were unlabeled (i.e., had neither the UBF nor the Nopp140 signal; NS-NPB). The frequency of these three NPB classes changed over  
260 the course of development (Fig. 2A). In the late 2-cell stage embryos, we observed two major classes of NPBs: those that displayed Nopp140 and UBF signals (~40%; n=44 nuclei) and those that were unlabeled (~60% per nuclei; n=44 nuclei). The percentage of unlabeled NPBs then significantly decreased from the 2-cell stage to the early 4-cell stage (~50%, n=48 nuclei, p<0.001, Kruskal-Wallis test) and the late 4-cell stage (~20%, n=49 nuclei, p<0.001, Kruskal-  
265 Wallis test). The third class of NPBs, with the Nopp140 signal only, was observed mainly during the early 8-cell stage ~25%, n=59 nuclei, Fig. 2A/B). By the late 8-cell stage (n=103 nuclei) and the early 16-cell stage (n=98 nuclei), there were no longer any unlabeled NPBs. The remaining

NPBs (on average two per nucleus, for both stages) displayed both Nopp140 and UBF signals. Finally, from the late 16-cell stage to the blastocyst stage, no NPBs (i.e. structures with a central core that showed no sign of DNA staining) were present (Fig. 1).

**UBF and NOPP140 distribution in early preimplantation embryos** Next, we focused on the distribution of UBF and Nopp140 proteins in Nopp140- and UBF-positive NPBs. In late 2-cell stage embryos (2cL, Fig. 1 upper panel), high-intensity UBF and Nopp140 signals were observed, co-localizing at the periphery of the NPBs. During the 4-cell stage, the Nopp140 signals became more diffuse and formed partial rings in the cortical region of the NPBs, while the UBF signals became more abundant and more heterogeneous in size (4cE and 4cL, Fig. 1 upper panel). The pattern observed during the early 8-cell stage was very similar to that observed during the late 4-cell stage, except that the Nopp140 rings were complete in the former (8cE, Fig. 1 upper panel). During the late 8-cell stage, the central core of the NPBs was clearly smaller in size and surrounded by a large, irregular zone that was slightly stained for DNA. Nopp140 signals were of greater intensity at the periphery of this zone, while UBF signals accumulated inside this zone and showed both a diffuse and punctuated distribution (8cL, Fig. 1 upper panel). From late 2-cell stage to 16-cell stage we could observe some UBF spots with greater intensity (for example: arrowhead in 8cE, Fig. 1 upper panel). The distributions of UBF and Nopp140 were similar in late 8-cell embryos and 16-cell embryos (16cE, Fig. 1 upper panel). Notably, the dark NPB cores shrank progressively as development progressed and disappeared entirely by the end of the 16-cell stage (16cL, Fig. 1 lower panel).

NPBs displaying Nopp140 signals occurred more frequently during the late 4-cell (12%,  $p=0.1$ , Kruskal-Wallis test) and early 8-cell (26%,  $p<0.001$ , Kruskal-Wallis test) stages (Fig. 2A/B).

During the late 4-cell stage, such NPBs were mostly very small and associated with large Nopp140 spots. During the early 8-cell stage, they were associated with large Nopp140 spots or rings.

In early morulae, the Nopp140 signals predominantly formed thick rings (~2 per nucleus) that encircled diffuse and punctuated UBF signals, a pattern similar to that seen in late 16-cell-stage embryos (Fig. 1 lower panel). Importantly, another pattern emerged at those stages: Nopp140 signals formed clusters that contained UBF signals (arrowhead in Fig. 1 lower panel). These clusters were seen in the late morula and blastocyst stages, both in ICM and trophectoderm cells (Fig. 1 lower panel). It is similar to the one that has been observed in the nucleoli of mouse somatic cells [27,47].

During all these developmental stages, we detected Nopp140 spots within the nucleoplasm, which were, for most of them, devoid of UBF signals (arrows in 8cE/8cL, Fig. 1 upper panel); with a maximum at the 16-cell stage (Fig. 2C). However sometimes these Nopp140 spots colocalized with UBF, especially at the 2-cell stage and from the 16-cell stage onwards (arrows in Early Morual, Fig.1 lower panel and Fig. 2C). These nucleoplasmic spots were close or even apposed to NPBs and most probably corresponded to Cajal bodies [23,36].

### **Interactions between UBF and NOPP140**

The immunofluorescent staining results suggest that UBF and Nopp140 proteins colocalize in the cortical region of the NPBs between the 2-cell and 16-cell stages and in the nucleoplasm at certain other stages. To test whether this reflects a true spatial proximity, we used a new in situ PLA technique. This sensitive approach can be utilized to confirm the presence of interactions between two spatially close proteins (i.e., when they are separated by less than 30–40 nm).

Protein-protein interactions are revealed by the presence of fluorescent spots [48–50]. In the PLA  
315 experiments, we observed high-intensity spots during all stages (Fig. 3). These spots were mostly  
localized at the periphery of the NPBs but were sometimes observed in the nucleoplasm (Fig. 3,  
z-sections). Importantly, the number of PLA spots gradually increased over the course of  
development, from approximately 2 spots in the late 2-cell stage to around 18 spots in the 16-cell  
stage (Fig. 3).

320

### **Impact of CX-5461-mediated RNA polymerase I inhibition on embryonic development**

Our results show that UBF and NOPP140 proteins are reorganized in the cortical region of NPBs  
over the course of development, from the late 2-cell stage, by which time rDNA transcription has  
started [17], up until the morula stage. To evaluate the relationship between these morphological  
325 and functional changes, we investigated whether UBF and Nopp140 reorganization was  
dependent on rDNA transcription. We used a novel synthetic inhibitor, CX-5461, which  
specifically inhibits RNA pol I [51]. First, we determined the effect of this inhibitor on  
embryonic development. One-cell stage embryos were collected and cultured at various  
concentrations of CX-5461 (80 nM, 300 nM, 500 nM, and 1  $\mu$ M; as previously tested on cells  
330 [42–44]). At CX-5461 concentrations of 80, 300, and 500 nM, embryos reached the blastocyst  
stage, but their morphological quality was quite poor (data not shown). Embryos cultured with 1  
 $\mu$ M CX-5461 never reached the blastocyst stage (Table 1). Treated embryos cleaved normally  
going from the 1-cell to the 2-cell stage (comparable to controls), but the cleavage needed to  
reach the 4-cell stage was delayed. Compared to 63% of the control embryos, only 42% of the  
335 treated embryos were at the 4-cell stage 28 hours after having been transferred into the culture  
drops containing CX-5461 (D2 +28H; statistically different with  $p < 0.001$ , Fisher test). The



percentage of 4-cell embryos in the treatment group climbed to 66% 20 hours later (D2 +48H), but none of them gave rise to 8-cell embryos (Table 1).

To check whether CX-5461's strong detrimental effects on development were indeed due to its inhibition of RNA pol I, we analyzed rDNA transcriptional activity in embryos treated with 1 $\mu$ M CX-5461. Such concentrations are supposed to reduce the rate of rDNA transcription in somatic cells by up to 90% [42]. We used BrUTP signaling to reveal patterns of rDNA transcription in control and CX-5461-treated late 2-cell-stage embryos [17]. As expected, 92% of control embryos contained large clusters of BrUTP signals in their NPBs (Fig. 4, Table 2). In contrast, in the treatment group, only 33% of embryos displayed BrUTP signals. Furthermore, BrUTP signaling was of lower intensity in the treated embryos than in the control embryos. Because the treated embryos developed more slowly (Table 1), we analyzed their rDNA transcription levels 4 hours later than for the control group (28 hours after transfer to the culture drops containing CX-5461). Although the percentage of BrUTP-positive embryos was higher in the treatment group (58%), the signals were of lower intensity (Fig. 4, Table 2). Taken together, these results confirm that CX-5461 inhibits embryonic rDNA transcription and development.

### **Impact of CX-5461-mediated RNA polymerase I inhibition on UBF and Nopp140 distribution**

Next, we examined the impact of CX-5461 on the localization patterns of UBF and Nopp140 using the immunofluorescent staining technique described above. We observed very distinct patterns in CX-5461-treated versus control embryos. In 2-cell embryos in the treatment group, Nopp140 was distributed all around the NPBs, forming rings containing few UBF signals (n=14 nuclei; D2 + 24H, Fig. 5). In 4-cell embryos in the treatment group (+28 hours and +48 hours after transfer to culture drops containing CX-5461; n=37 and 118, respectively), large UBF spots

surrounded by Nopp140 signals were regularly observed forming concave structures or “caps” (arrowheads in Fig. 5). In addition, we also often observed nuclear protrusions (arrows in Fig. 5) in CX-5461-treated embryos, which underscores their poor morphological quality.

In transcriptionally inactive oocytes Zatssepina et al. [52] have observed RNA pol I/UBF foci localized at the periphery of the nucleolus-like bodies (NLBs). We thus co-immunostained transcriptionally inactive oocytes using anti-Nopp140 and anti-UBF antibodies. We observed in these oocytes similar Nopp140/UBF "caps" at the periphery of the NLBs (Fig. 5; n=11) as in the 4-cell treated embryos. This suggests that "caps" are a consequence of transcriptional inhibition resulting from the segregation of nucleolar components, as has been observed in somatic cells inhibited with actinomycin-D [41,53].

We therefore analyzed rDNA transcription in relation to the distribution of UBF and Nopp140 proteins by double immuno-RNA FISH with a probe that specifically binds to the 5'-external transcribed spacer (5'ETS) of the 47S pre-rRNA transcript. In 4-cell embryos Nopp140, UBF and 5'ETS showed a peculiar distribution : the 5'ETS signal was less diffuse and juxtaposed to Nopp140-UBF "caps" in the treatment group whereas it formed in the control embryos thick rings in which Nopp140 and UBF signals were embedded (Fig 6). Moreover, the 5'ETS signal was of much lower intensity in the treated embryos than in the control embryos (Fig. 6). Because immunostainings for UBF and Nopp140 look alike in transcriptionally inactive oocytes (Fig. 5) we also performed immuno-RNA FISH on oocytes. Notably, the immuno-RNA FISH signal observed in the transcriptionally inactive oocytes was quite similar to the one observed in treated embryos (Fig. 6).

Taken together, these results confirm that inhibition of rDNA transcription in early embryos by CX-5461 is accompanied by a profound reorganization of UBF and Nopp140.

## Discussion

385 The aim of our study was to analyze in details nucleologenesis in mouse preimplantation embryos . This study is the first to describe the distribution of both UBF and Nopp140 from the 2-cell through the blastocyst stage.

### **NPB heterogeneity between the 2-cell stage and the early 8-cell stage**

The first striking characteristic of early embryonic development is that NPBs were 390 heterogeneously associated with UBF and Nopp140 Zatsepina et al. [17] have proposed that unlabeled NPBs (NS-NPB) could either lack associations with chromosomes bearing rDNA sequences or form associations with inactive ribosomal genes. FISH experiments on 1- and 2-cell embryos have shown that not all NPBs are associated with rDNA ([54,55]; our unpublished data). We could thus assume that the NS-NPB population observed in our study at late 2-cell stage are 395 not associated with ribosomal genes.

This heterogeneity in the Nopp140 and UBF signals, also raises questions about the different possible contents and functions of the different NPBs. Biggiogera et al. [21] showed that NPBs contain RNA, fibrillarin, and other components, such as ribosomal proteins, heterogeneous nuclear ribonucleoproteins, and nucleoplasmic small nuclear ribonucleic proteins; however, they 400 did not analyze whether these components were present in all NPBs. Thus, even if two different groups [25,56] have recently observed B23/nucleoplasmin; C23/nucleolin and fibrillarin in all the NPBs from the 1-cell to the blastocyst, we can suggest that the NPBs displaying no UBF signal may serve to store other nucleolar components.

In addition, the percentage of NPBs not displaying a UBF signal significantly decreased within 405 stages and over the course of development (Fig. 2B). These NPBs may be equivalent to the

heterogeneous prenucleolar bodies (PNBs) of various composition that have been observed at the beginning of interphase in somatic cells [9,57,58] and that rapidly fuse to form nucleoli. NPB fusion has indeed already been amply documented in embryos [17,59].

Starting at the late 8-cell stage, NPBs with both Nopp140 and UBF signals were fairly pervasive, suggesting that all the NPBs present from this point on are involved in rRNA production and early processing. This supports the recent publication by Lavrentyeva et al. [56] showing accumulation of processed pre-rRNA in NPBs in embryos with more than 4 cells.

### **UBF and Nopp140 distributions diverge rapidly after the onset of transcription**

During the late 2-cell and 4-cell stages, the localization of UBF and Nopp140 around the periphery of the NPBs is consistent with that previously observed by Baran et al. [23] and Zatssepina et al. [17]. The latter further showed that UBF spots are associated with new rRNA transcripts. These spots were quite large in these earlier stages, suggesting that several transcription units were concentrated at the same point and that the chromatin was still quite structurally compact. As Nopp140 has been shown to interact with snoRNPs [38,39], each UBF/Nopp140 spot could correspond to one ribosomal transcription and early processing site. If so, the rings of UBF signals that formed around the NPBs may represent active tandemly repeated rDNA sequences.

Thereafter, patterns of protein distribution changed drastically. Starting at the 8-cell stage, the area occupied by the two proteins at the periphery of the NPBs expanded, and the dark NPB core gradually diminished in size, disappearing by the late 16-cell stage, thus allowing UBF to occupy the center of the former NPB, while Nopp140 formed a thick ring of great intensity at its periphery. This redistribution parallels the ultrastructural modifications that have been described in mouse embryos using electron microscopy: a reticulation process starts at the NPB periphery

and includes the emergence of intermingled fibrillar and granular compartments [13,15,19,20].  
430 This process gives rise to a nucleolonema, which corresponds to the fibrillar part of the  
reticulated structure that emerges from the NPB cortex. Geuskens and Alexandre [20] further  
showed that rDNA is transcribed in the fibrillar part of this reticulated peripheral structure and  
that the nascent rRNA is then transported to the granular part. Our results are consistent with  
these findings.

435 We never observed any Nopp140 or UBF signals in the core of the NPBs, which is consistent  
with results from other studies of mouse embryos that examined the localization of other  
nucleolar proteins using immunostaining [17,22,24,60–62]. However, several authors [15,24],  
using immunoelectron microscopy, have shown that some nucleolar proteins are present in the  
inner core of NPBs from the 1-cell to the 8-cell stage. It should be pointed out, though, that Fulka  
440 and Langerova [25] recently detected nucleolar proteins, including UBF, in the NPB core using  
an antigen retrieval technique. Thus, the lack of signaling in the central core of NPBs does not  
mean that Nopp140 and UBF were indeed absent from the region.

Finally, during the late morula stage, the NPBs disappeared and the Nopp140 and UBF signals  
intermingled in three to six large clusters that were clumped together (Fig. 1 lower panel). This  
445 pattern is very similar to the one observed in the nucleoli of somatic cells [26,27].

### **Nopp140 nucleoplasmic foci**

We also detected Nopp140 signals in the nucleoplasm, generally in close proximity to the NPBs,  
which fits with the findings of Baran et al. [23]. Because there is ample evidence that Nopp140  
interacts with coilin [35–37,63], our results strongly suggest that these nucleoplasmic foci are  
450 Cajal (coiled) bodies [64]. Moreover, Nopp140 has been described as a chaperone of the

snRNPs involved in rRNA processing and, as such, it should shuttle between the nucleolus and the coiled bodies [37–39]. Our findings support this idea .

Surprisingly, the number of Nopp140 nucleoplasmic spots increased dramatically up until the late 16-cell stage and then decreased (Fig 2C). Previous studies have shown that Cajal body number  
455 increases when cells are stimulated to grow rapidly or when high levels of gene expression are induced [63,65]. It may also be due to the fact that these highly dynamic structures undergo regulated cycles of assembly and disassembly [66–68]. Consequently, it could be informative to analyze their size distribution.

### **Interactions between UBF and Nopp140**

460 Using the highly sensitive PLA (Duolink) technique, we were able to detect molecular interactions between UBF and Nopp140 (i.e., a distance of less than 40 nm). Interestingly, the number of spots per nucleus became significant at late 4-cell stage and increased up to the 16-cell stage. It should be noted that we quantified the total number of spots regardless of their localization as DNA staining in PLA assay was not good enough to allow a precise  
465 discrimination of NPBs. However PLA spot seem to be more abundant around NPBs (z-section images in Fig. 4) and could be linked to several processes. First, Nopp140 and UBF have been found to be localized in both the FC and the DFC [26,27], which are intermingled [7,9,57,69,70]. The 3D intermingling of these two NPB compartments could result in the close spatial proximity of these two proteins. Second, UBF is a component of the RNA pol I holoenzyme [6,30] and it  
470 has been shown that Nopp140 colocalizes with RNA pol I [23,71]. Indeed, it interacts with RPA subunit 194 [41] and casein kinase II, which also belongs to the RNA pol I transcriptional machinery [40,41,72]. Thus, the spatial organization of the holoenzyme components could result in the close spatial proximity of UBF and Nopp140. Third, Nopp140 and other factors that form

part of the pre-rRNA processing machinery are known to associate with rDNA outside of rRNA  
475 synthesis, and UBF is necessary for the recruitment process [10]. Maden [73] and Yang et al.  
[38] have also suggested that transcription and processing could occur simultaneously. In this  
case, complexes and proteins involved in these two steps of ribosomal biogenesis could be  
grouped at rDNA transcription sites and thus be close enough to interact with each other.

On the other hand, some PLA spots were also observed in the nucleoplasm. We believe these  
480 could correspond to the few putative coiled bodies displaying both Nopp140 and UBF signals as  
observed by immunodetection (Fig. 4C). Indeed, it has been shown that factors forming part of  
the RNA pol I machinery are present in the Cajal bodies [74] ; however, UBF's presence is very  
transient because it is rapidly recruited to the nucleoli [75]. Whereas this colocalisation was not  
often visible by immunodetection, we most probably caught this transient event with the PLA  
485 procedure due to the 2-hours amplification step.

### **RNA polymerase I inhibition by CX-5461**

To analyze the link between nucleologenesis and rDNA transcription, we used CX-5461 to  
specifically inhibit RNA pol I activity Embryos treated with 0.5  $\mu$ M CX-5461 reached the  
blastocyst stage (27%; n=15), which contrasts with previous findings that 0.5  $\mu$ M of CX-5461  
490 can block the embryos in the 1-cell stage [76]. This discrepancy could be explained by  
methodological differences: i) the fertilization procedure used (natural mating versus IVF); ii) the  
time of exposure to the drug (24 hphCG versus fertilization); and iii) the solution used to  
resuspend the drug ( $\text{NaH}_2\text{PO}_4$  versus DMSO). Anyway, we observed blastocysts of poor quality.

Treatment with 1 $\mu$ M CX-5461 led to a decrease in the number of 2-cell embryos engaged in  
495 rDNA transcription, as well as lower-intensity signaling and a more diffuse distribution of  
transcription sites as revealed by BrUTP incorporation and RNA FISH. Our data concur with

those of Drygin et al. [42], who showed that 1 $\mu$ M CX-5461 can considerably reduce the ribosomal gene transcription rate (90%). The small amount of residual transcription observed in the embryos suggests that a few sites are still active but are functioning at lower levels. In addition, the increase in the number of 2-cell embryos transcribing between 24 and 28 hours after transfer to the culture drops containing CX-5461 could reflect a delay in the initiation of ribosomal gene transcription. In any case, the low transcription levels in CX-5461-treated embryos could be related to the developmental delay and arrest observed at the 4-cell stage.

Recently Lavrentyeva et al. [56] have shown by RNA-FISH that 1-cell embryos are significantly impoverished for RNA and that in late 2-cell embryos nascent rRNAs appear on NPB surface, supporting our results. Moreover, we confirmed here by immuno-RNA FISH that the UBF and Nopp140 are indeed localized at the initiation sites of rRNA synthesis on the NPB surface in 4-cell embryos.

More interestingly, we observed that the CX-5461 treatment led to a reorganization of nucleolar components at both the 2- and 4-cell stages. In particular, in 4-cell treated embryos, Nopp140 and UBF formed “nucleolar caps.” Those caps correspond to those observed in transcriptionally inactive oocytes (Fig. 5 & 6) [52]. Similar distributions of Nopp140 and UBF have also been observed during interphase in the nucleoli of actinomycin-D-treated somatic cells [41,53,77]. These findings strongly suggest that the inhibition of ribosomal transcription leads to the reorganization of nucleolar proteins and probably that of the nucleolar compartment.

Taken together, these data suggest that i) the structural organization of nucleoli in the mouse embryo is tightly linked to RNA pol I transcription and ii) ribosomal transcription is essential for long-term development.





**Acknowledgements**

We thank Prof. U. Thomas Meier and Dr. Marie Françoise O'Donohue for their scientific support. We are grateful to Claire Boulesteix and Tiphaine Aguirre-Lavin for their help in running the lab. We also acknowledge Pierre Adenot and the platform MIMA2 (Microscopie et Imagerie des Microorganismes, Animaux et Elements) for microscopy equipment as well as UE IERP for animal care (Unité Expérimentale d'Infectiologie Expérimentale des Rongeurs et Poissons).

## REFERENCES

- [1] Bultman SJ, Gebuhr TC, Pan H, Svoboda P, Schultz RM, Magnuson T. Maternal BRG1 regulates zygotic genome activation in the mouse. *Genes Dev* 2006; 20:1744–1754.
- [2] Schultz RM. The molecular foundations of the maternal to zygotic transition in the preimplantation embryo. *Hum Reprod Update* 2002; 8:323–331.
- [3] Minami N, Suzuki T, Tsukamoto S. Zygotic gene activation and maternal factors in mammals. *J Reprod Dev* 2007; 53:707–715.
- [4] Lo SJ, Lee C-C, Lai H-J. The nucleolus: reviewing oldies to have new understandings. *Cell Res* 2006; 16:530–538.
- [5] Boisvert F-M, van Koningsbruggen S, Navascués J, Lamond AI. The multifunctional nucleolus. *Nature* 2007; 8:574–585.
- [6] Raška I, Kobema K, Malínský J, Fidlerová H, Mašata M. The nucleolus and transcription of ribosomal genes. *Biol Cell* 2004; 96:579–594.
- [7] Derenzini M, Pasquinelli G, O’Donohue M-F, Ploton D, Thiry M. Structural and functional organization of ribosomal genes within the mammalian cell nucleolus. *J Histochem Cytochem* 2006; 54(2):131–145.
- [8] Hernandez-Verdun D, Roussel P, Thiry M, Sirri V, Lafontaine DLJ. The nucleolus: structure/function relationship in RNA metabolism. *Wiley Interdiscip Rev RNA* 2010; 1:415–431.
- [9] Hernandez-Verdun D. The nucleolus: a model for the organization of nuclear functions. *Histochem Cell Biol* 2006; 126:135–148.
- [10] Ueshima S, Nagata K, Okuwaki M. Upstream binding factor-dependent and pre-rRNA transcription-independent association of pre-rRNA processing factors with rRNA gene. *Biochem Biophys Res Commun* 2014; 443:22–27.
- [11] Engel W, Zenzes MT, Schmid M. Activation of mouse ribosomal RNA genes at the 2-cell stage. *Hum Genet* 1977; 38:57–63.
- [12] Kobema K, Landa V, Kaňka J, Pliss A, Eltsov M, Staněk D, Raška I. Non-isotopic detection of nucleolar transcription in pre-implantation mouse embryos To cite this version □: Non-isotopic detection of nucleolar transcription. *Reprod Nutr Dev* 1998; 38:117–126.
- [13] Takeushi, IK and Takeushi YK. Ultrastructural Localization of Ag-NOR Proteins in Full-Grown Oocytes and Preimplantation Embryos of Mice Ikuo K. *J Electron Microscop* (Tokyo) 1986; 35:280–287.
- [14] Fléchon JE, Kopečný V. The nature of the ‘nucleolus precursor body’ in early preimplantation embryos: a review of fine-structure cytochemical, immunocytochemical and autoradiographic data related to nucleolar function. *Zygote* 1998; 6:183–91.
- [15] Biggiogera M, Bürki K, Kaufmann SH, Shaper JH, Gas N, Amalric F. Nucleolar distribution of proteins B23 and nucleolin in mouse preimplantation embryos as visualized by immunoelectron microscopy. *Development* 1990; 1270:1263–1270.
- [16] Prather R, Simerly C, Schatten G, Pilch DR, Lobo SM, Marzluff WF, Dean WL, Schultz G a. U3 snRNPs and nucleolar development during oocyte maturation, fertilization and early embryogenesis in the mouse: U3 snRNA and snRNPs are not regulated coordinate with other snRNAs and snRNPs. *Dev Biol* 1990; 138:247–55.
- [17] Zatsepina O, Baly C, Chebrout M, Debey P. The Step-Wise Assembly of a Functional Nucleolus in Preimplantation Mouse Embryos Involves the Cajal ( Coiled ) Body. *Dev Biol* 2003; 83:66–83.
- [18] Piko L, Clegg KB. Quantitative Changes in Total RNA, Total Poly (A), and Ribosomes

- in Early Mouse Embryos. *Dev Biol* 1982; 89:362–378.
- [19] Fakan S, Odartchenko N. Ultrastructural organization of the cell nucleus in early mouse embryos. *Biol Cell* 1980; 37:211–217.
- [20] Geuskens M, Alexandre H. Ultrastructural and autoradiographic studies of nucleolar development and rDNA transcription in preimplantation mouse embryos. *Cell Differ* 1984; 14:125–134.
- [21] Biggiogera M, Martin T., Gordon J, Amalric F, Fakan S. Physiologically Inactive Nucleoli Contain Nucleoplasmic Ribonucleoproteins: Immunoelectron Microscopy of Mouse Spermatids and Early Embryos. *Exp Cell Res* 1994; 213:55–63.
- [22] Baran V, Veselá J, Reháč P, Koppel J, Fléchon J. Localization of fibrillarin and nucleolin in nucleoli of mouse preimplantation embryos. *Mol Reprod Dev* 1995; 40:305–310.
- [23] Baran V, Brochard V, Renard J-P, Flechon JE. Nopp 140 involvement in nucleologenesis of mouse preimplantation embryos. *Mol Reprod Dev* 2001; 59:277–84.
- [24] Cuadros-Fernández JM, Esponda P. Immunocytochemical localisation of the nucleolar protein fibrillarin and RNA polymerase I during mouse early embryogenesis. *Zygote* 1996; 4:49–58.
- [25] Fulka H, Langerova A. The maternal nucleolus plays a key role in centromere satellite maintenance during the oocyte to embryo transition. *Development* 2014; 141:1694–1704.
- [26] Roussel P, André C, Masson C, Géraud G, Hernandez-verdun D, Hématologie-immunologie C, Mondor HH. Localization of the RNA polymerase I transcription factor hUBF during the cell cycle. *J Cell Sci* 1993; 337:327–337.
- [27] Thiry M, Cheutin T, Lamaye F, Thelen N, Meier UT, Donohue MO, Ploton D. Localization of Nopp140 within mammalian cells during interphase and mitosis. *Histochem Cell Biol* 2009; 132:129–140.
- [28] Jantzen HM, Admon a, Bell SP, Tjian R. Nucleolar transcription factor hUBF contains a DNA-binding motif with homology to HMG proteins. *Nature* 1990; 344:830–836.
- [29] Panov KI, Friedrich JK, Russell J, Zomerdijk JCBM. UBF activates RNA polymerase I transcription by stimulating promoter escape. *Embo J* 2006; 25:3310–3322.
- [30] Grummt I. Life on a planet of its own: regulation of RNA polymerase I transcription in the nucleolus. *Genes Dev* 2003; 17:1691–1702.
- [31] Grummt I. Wisely chosen paths – regulation of rRNA synthesis. *FEBS J* 2010; 277:4626–4639.
- [32] Russell J, Zomerdijk JCBM. The RNA polymerase I transcription machinery. *Biochem Soc* 2006; 73:203–216.
- [33] Sanij E, Hannan RD. The role of UBF in regulating the structure and dynamics of transcriptionally active rDNA chromatin. *Epigenetics* 2009; 4:374–382.
- [34] Meier UT. A nuclear localization signal binding protein in the nucleolus. *J Cell Biol* 1990; 111:2235–2245.
- [35] Meier UT, Blobel G. Nopp140 shuttles on tracks between nucleolus and cytoplasm. *Cell* 1992; 70:127–138.
- [36] Meier U., Blobel G. NAP57, a mammalian nucleolar protein with a putative homolog in yeast and bacteria. *J Cell Biol* 1994; 127:1505–1514.
- [37] Isaac C, Yang Y, Meier UT. Nopp140 Functions as a Molecular Link Between the Nucleolus and the Coiled Bodies. *J Cell Biol* 1998; 142:319–329.
- [38] Yang Y, Isaac C, Wang C, Meier UT. Conserved Composition of Mammalian Box H / ACA and Box C / D Small Nucleolar Ribonucleoprotein Particles and Their Interaction with the Common Factor Nopp140. *Mol Biol Cell* 2000; 11:567–577.

- [39] Wang C, Query CC, Meier UT. Immunopurified Small Nucleolar Ribonucleoprotein Particles Pseudouridylate rRNA Independently of Their Association with Phosphorylated Nopp140. *Mol Cell Biol* 2002; 22:8457–8466.
- [40] Li D, Meier UT, Dobrowolska G, Krebs EG. Specific Interaction between Casein Kinase 2 and the Nucleolar Protein Nopp140. *J Biol Chem* 1997; 272:3773–3779.
- [41] Chen H, Pai C, Huang J, Chen H, Pai C, Huang J. Human Nopp140 , Which Interacts with RNA Polymerase I : Implications for rRNA Gene Transcription and Nucleolar Structural Organization Human Nopp140 , Which Interacts with RNA Polymerase I : Implications for rRNA Gene Transcription and Nucleolar Structura. *Mol Cell Biol* 1999; 19:8536–8546.
- [42] Drygin D, Lin a., Bliesath J, Ho CB, O'Brien SE, Proffitt C, Omori M, Haddach M, Schwaebe MK, Siddiqui-Jain a., Streiner N, Quin JE, et al. Targeting RNA Polymerase I with an Oral Small Molecule CX-5461 Inhibits Ribosomal RNA Synthesis and Solid Tumor Growth. *Cancer Res* 2011; 71:1418–1430.
- [43] Bywater MJ, Poortinga G, Sanij E, Hein N, Peck A, Cullinane C, Wall M, Cluse L, Drygin D, Anderes K, Huser N, Proffitt C, et al. Inhibition of RNA polymerase I as a therapeutic strategy to promote cancer-specific activation of p53. *Cancer Cell* 2012; 22:51–65.
- [44] Haddach M, Schwaebe MK, Michaux J, Nagasawa J, O'Brien SE, Whitten JP, Pierre F, Kerdoncuff P, Darjania L, Stansfield R, Drygin D, Anderes K, et al. Discovery of CX-5461, the first direct and selective inhibitor of RNA polymerase I, for cancer therapeutics. *ACS Med Chem Lett* 2012; 3:602–606.
- [45] Kent T, Lapik YR, Pestov DG. The 5' external transcribed spacer in mouse ribosomal RNA contains two cleavage sites. *RNA* 2009; 15:14–20.
- [46] Bouniol-Baly C, Hamraoui L, Guibert J, Beaujean N, Szöllösi MS, Debey P. Differential transcriptional activity associated with chromatin configuration in fully grown mouse germinal vesicle oocytes. *Biol Reprod* 1999; 60:580–587.
- [47] Sharma P, Murillas R, Zhang H, Kuehn MR. N4BP1 is a newly identified nucleolar protein that undergoes SUMO-regulated polyubiquitylation and proteasomal turnover at promyelocytic leukemia nuclear bodies. *J Cell Sci* 2010; 123:1227–1234.
- [48] Hervouet E, Vallette F, Cartron P. Dnmt3/transcription factor interactions as crucial players in targeted DNA methylation. *Epigenetics* 2009; 4(7):487–499.
- [49] Naegel K., White F., Lauffenburger D., Yaffe M. Robust co-regulation of tyrosine phosphorylation sites on proteins reveals novel protein interactions. *Mol Biosyst* 2012; 8:2771–2782.
- [50] Choo YY, Hagen T. Mechanism of Cullin3 E3 Ubiquitin Ligase Dimerization. *PLoS One* 2012; 7:1–8.
- [51] Drygin D, Rice WG, Grummt I. The RNA polymerase I transcription machinery: an emerging target for the treatment of cancer. *Annu Rev Pharmacol Toxicol* 2010; 50:131–56.
- [52] Zatssepina O V, Bouniol-baly C, Amirand C, Debey P. Functional and Molecular Reorganization of the Nucleolar Apparatus in Maturing Mouse Oocytes. *Dev Biol* 2000; 370:354–370.
- [53] Shav-tal Y, Blechman J, Darzacq X, Montagna C, Dye BT, Patton JG, Singer RH, Zipori D. Dynamic Sorting of Nuclear Components into Distinct Nucleolar Caps during Transcriptional Inhibition. *Mol Biol Cell* 2005; 16:2395–2413.
- [54] Aguirre-Lavin T, Adenot P, Bonnet-Garnier A, Lehmann G, Fleurot R, Boulesteix C, Debey P, Beaujean N. 3D-FISH analysis of embryonic nuclei in mouse highlights several abrupt changes of nuclear organization during preimplantation development. *BMC Dev Biol* 2012; 12:30.

- [55] Romanova L, Korobova F, Noniashvilli E, Dyban A, Zatsepina O. High Resolution Mapping of Ribosomal DNA in Early Mouse Embryos by Fluorescence Collection of Embryos. *Biol Reprod* 2006; 815:807–815.
- [56] Lavrentyeva E, Shishova AK, Kagarlitsky A., Zatsepina O. Localisation of RNAs and proteins in nucleolar precursor bodies of early mouse embryos. *Reprod Fertil Dev* 2015; (in press):Published online ahead of print 17 September 2015;
- [57] Hernandez-verdun D. Nucleolus: from structure to dynamics. *Histochem Cell Biol* 2006; 125:127–137.
- [58] Hernandez-Verdun D. Assembly and disassembly of the nucleolus during the cell cycle. *Nucleus* 2011; 2:189–194.
- [59] Kyogoku H, Fulka J, Wakayama T, Miyano T. De novo formation of nucleoli in developing mouse embryos originating from enucleolated zygotes. *Development* 2014; 141:2255–2259.
- [60] Ferreira J, Carmo-fonseca M. The biogenesis of the coiled body during early mouse development. *Development* 1995; 612:601–612.
- [61] Romanova LG, Anger M, Zatsepina O V, Schultz RM. Implication of nucleolar protein SURF6 in ribosome biogenesis and preimplantation mouse development. *Biol Reprod* 2006; 75:690–696.
- [62] Vogt EJ, Meglicki M, Hartung KI, Borsuk E, Behr R. Importance of the pluripotency factor LIN28 in the mammalian nucleolus during early embryonic development. *Development* 2012; 139:4514–23.
- [63] Ogg SC, Lamond A. Cajal bodies and coilin--moving towards function. *J Cell Biol* 2002; 159:17–21.
- [64] Raska I, Andrade LE, Ochs RL, Chan EK, Chang CM, Roos G, Tan EM. Immunological and ultrastructural studies of the nuclear coiled body with autoimmune antibodies. *Exp Cell Res* 1991; 195:27–37.
- [65] Morris GE. The Cajal body. *Biochim Biophys Acta* 2008; 1783:2108–2115.
- [66] Carmo-Fonseca M, Ferreira J, Lamond AI. Assembly of snRNP-containing coiled bodies is regulated in interphase and mitosis--evidence that the coiled body is a kinetic nuclear structure. *J Cell Biol* 1993; 120:841–52.
- [67] Lamond AI, Carmo-Fonseca M. The coiled body. *Trends Cell Biol* 1993; 3:198–204.
- [68] Platani M, Goldberg I, Swedlow JR, Lamond AI. In vivo analysis of Cajal body movement, separation, and joining in live human cells. *J Cell Biol* 2000; 151:1561–1574.
- [69] Sirri V, Urcuqui-inchima S, Hernandez-verdun D, Roussel P. Nucleolus□: the fascinating nuclear body. *Histochem Cell Biol* 2008; 129:13–31.
- [70] Bártová E, Harni A, Uhlí R, Ra I, Galiová G, Orlova D, Kozubek S. Structure and Epigenetics of Nucleoli in Comparison With Non-nucleolar Compartments. *J Histochem Cytochem* 2010; 58:391–403.
- [71] Tsai Y-T, Lin C-I, Chen H-K, Lee K-M, Hsu C-Y, Yang S-J, Yeh N-H. Chromatin tethering effects of hNopp140 are involved in the spatial organization of nucleolus and the rRNA gene transcription. *J Biomed Sci* 2008; 15:471–486.
- [72] Meier UT. Comparison of the rat nucleolar protein nopp140 with its yeast homolog SRP40. Differential phosphorylation in vertebrates and yeast. *J Biol Chem* 1996; 271:19376–84.
- [73] Maden B. The numerous modified nucleotides in eukaryotic ribosomal RNA. *Prog Nucleic Acid Res Mol Biol* 1990; 39:241–303.
- [74] Gall JG, Bellini M, Wu Z, Murphy C. Assembly of the Nuclear Transcription and Processing Machinery□: Cajal Bodies ( Coiled Bodies ) and Transcriptosomes. *Mol Biol Cell* 1999; 10:4385–4402.

- [75] Dundr M, Hebert MD, Karpova TS, Stanek D, Xu H, Shpargel KB, Meier UT, Neugebauer KM, Matera AG, Misteli T. In vivo kinetics of Cajal body components. *J Cell Biol* 2004; 164:831–842.
- [76] Lin C-J, Koh F., WONG P, Conti M, Ramalho-Santos M. Hira-mediated H3.3 incorporation is required for DNA replication and ribosomal RNA transcription in the mouse zygote. *Dev Cell* 2015; 30:268–279.
- [77] Dousset T, Wang C, Chen D. Initiation of Nucleolar Assembly Is Independent of RNA Polymerase I Transcription. *Mol Cell Biol* 2000; 11:2705–2717.

## FIGURE LEGENDS

### **Figure 1. Distributions of Nopp140 and UBF in mouse embryos during preimplantation development (late 2-cell to blastocyst stage)**

Single representative confocal z-sections of embryos produced by natural fertilization and stained for DNA (blue), Nopp140 (red), and UBF (green); the merged colors are in the last row of each panel. Embryos were fixed either early (E) or late (L) in each stage from the 2-cell [2c] to the morula stage. At the blastocyst stage, examples of cells from the inner cell mass (ICM) or the trophectoderm (TE) are shown. At the 8-cell stage [8c], an example of high-intensity nucleolar UBF spot that demonstrated only light Nopp140 staining is indicated by a single arrowhead and Nopp140 spots in the UBF-devoid nucleoplasm are indicated by arrows (upper panel). In the early morulae, Nopp140/UBF spots present in the nucleoplasm are indicated by arrows and clusters of Nopp140 proteins that colocalized with UBF proteins are indicated by a single arrowhead (lower panel). Scale bar: 10  $\mu$ m.

Full 3D-projections of some of the analyzed embryos are shown in the bottom right column to illustrate the homogeneity observed between cells within each embryo (PB: Polar Body). In morula, two cells that are in mitosis (arrowheads) do not present any Nopp140 signal but only some UBF spots that remain bound to chromosomes, as expected [17].

### **Figure 2. Statistical analysis of Nopp140 and UBF signals**

Images were analyzed, section by section through the entire confocal z-stack, and several criteria were evaluated in as many nuclei as possible for each embryo. The two upper panels show the frequency (panel A) and proportion (panel B) of NPBs per cell according to their Nopp140 and UBF signals during early development (from late 2-cell stage [2cL] to early 16-cell stage [16cE]). Black bars: NPBs displaying both Nopp140 and UBF signals [Nopp140/UBF-NPB]; gray bars: NPBs displaying a Nopp140 signal only [Nopp140 -NPB];



white bars: NPBs with no signals [NS-NPB]. Mean values  $\pm$  standard errors are given. Bars with different superscripts (a,b,c,d / e,f / g,h) indicate significantly different values between developmental stages within each type of NPB ( $p < 0.001$ ; Kruskal-Wallis test).

Panel C: Images were analysed, section by section through the entire confocal z-stack, and the number of Nopp140 nucleoplasmic spots with or without tandem UBF signals (continuous line vs. dotted line, respectively) were evaluated in as many nuclei as possible for each embryo from late 2-cell stage [2cL] to early blastocyst stage [BlastE]. Mean values  $\pm$  standard errors are given.

For all panels, the total number of nuclei analyzed are indicated. As many nuclei as possible were analyzed per embryo for each developmental stage: 2cL n=23 embryos, 4cE n=13 embryos; 4cL n=17 embryos; 8cE n=8 embryos; 8cL n=15 embryos; 16cE n=7 embryos; 16L n=8 embryos; MorulaE n=11 embryos; MorulaL n=12 embryos; BlastE n=15 embryos.

**Figure 3. Interactions between UBF and Nopp140 at different developmental stages as detected using a proximity ligation assay technique**

The green fluorescent dots indicate that the distance between UBF and Nopp140 was less than 30–40 nm. The proteins demonstrated this degree of proximity during all the stages studied, from the late 2-cell (2cL) stage to the early 16-cell (16cE) stage. DNA is stained in red. The upper row images are projections of all the z-sections and the lower row corresponds to single representative z-sections (apoptome) showing that colocalization mostly occurred near the NPBs. Scale bar: 10  $\mu$ m.

The boxplots on the right hand show the number of fluorescent dots obtained. The asterisks indicate when a significant difference was found ( $p < 0.001$ ; Kruskal-Wallis test) between two consecutive stages. The number of nuclei analyzed per stage is indicated. As many nuclei as possible were analyzed per embryos for each developmental stage: 2cL n=25 embryos, 4cE

n=24 embryos; 4cL n=22 embryos; 8cE n=22 embryos; 8cL n=14 embryos; 16cE n=23 embryos.

**Figure 4. Pol I-dependent transcription in control and CX-5461-treated late 2-cell-stage embryos**

Representative images (Apotome single z-sections) of transcription after BrUTP microinjections in control and CX-5461-treated embryos. DNA was counterstained with DAPI (blue). The BrUTP signal (green) was much less diffuse and of lower intensity in the CX-5461-treated embryos than in the control embryos; sometimes it was even absent. Scale bar: 10  $\mu$ m.

**Figure 5. Impact of the CX-5461 treatment on UBF and Nopp140 distributions**

Representative images of CX-5461-treated embryos at various time points after their transfer to drops containing the inhibitor (three upper rows) and of transcriptionally inactive oocytes (last row). DNA is stained blue, Nopp140 is stained red, and UBF is stained green. Whole embryo projections are shown in the first column, and enlarged single z-sections are shown in the other three columns (the corresponding nuclei are indicated on the projection). The Nopp140 and UBF “caps” are indicated by arrowheads, and the nuclear protrusions are indicated by arrows. PB: polar body. Scale bar: 10  $\mu$ m.

**Figure 6: Impact of the CX-5461 treatment on rDNA transcription and UBF-Nopp140 distributions**

Representative images of 4-cell control embryos (56hphCG) and CX-5461-treated embryos (D2 +48h after their transfer to drops containing the inhibitor) and of transcriptionally

inactive oocytes. Ribosomal RNA transcription was detected by RNA-FISH with a 5'ETS probe in white, Nopp140 is stained red, and UBF is stained green. Single z-sections with the 5'ETS signal alone are shown in the upper row and Nopp140/UBF signals are shown in the second row (with blue DNA counterstaining). The last row corresponds to the merged immuno-RNA FISH. Scale bar: 5  $\mu$ m.

**Table 1: Development of embryos upon transfer into culture drops (Day 1, T0) with 1 $\mu$ M CX-5461 or without (control).** Development was evaluated every day (D1 up to D5) and the number of embryos at each stage (as well as the corresponding percentage) are indicated. Three different experiments were pooled.

		D (T0)	D2 (+24H)	D2 (+28H)	D3 (+48H)	D3 (+52H)	D4 (+72H)	D5 (+96H)
<b>CONTROL</b>	<b>1-cell</b>	<b>104 (100%)</b>	<b>6 (6%)</b>	<b>5 (5%)</b>	<b>4 (4%)</b>	<b>3 (3%)</b>	<b>3 (3%)</b>	<b>3 (3%)</b>
	<b>2-cell</b>		<b>98 (94%)</b>	<b>31 (32%)</b>	<b>2 (2%)</b>	<b>1 (1%)</b>	<b>1 (1%)</b>	<b>1 (1%)</b>
	<b>4-cell</b>			<b>68 (63%)</b>	<b>7 (6%)</b>	<b>3 (3%)</b>	<b>3 (3%)</b>	<b>3 (3%)</b>
	<b>8-cell</b>				<b>91 (88%)</b>	<b>17 (16%)</b>	<b>3 (3%)</b>	<b>3 (3%)</b>
	<b>16-cell</b>					<b>80 (77%)</b>	<b>12 (11%)</b>	<b>2 (2%)</b>
	<b>Morula</b>						<b>60 (56%)</b>	<b>-</b>
	<b>Blastocyst</b>						<b>22 (23%)</b>	<b>92 (88%)</b>
<b>CX-5461</b>	<b>1-cell</b>	<b>78 (100%)</b>	<b>28 (32%)</b>	<b>28 (32%)</b>	<b>18 (20%)</b>	<b>18 (20%)</b>	<b>18 (20%)</b>	<b>18 (20%)</b>
	<b>2-cell</b>		<b>50 (68%)</b>	<b>21 (26%)</b>	<b>12 (13%)</b>	<b>12 (13%)</b>	<b>12 (13%)</b>	<b>12 (13%)</b>
	<b>4-cell</b>			<b>29 (42%)</b>	<b>48 (66%)</b>	<b>48 (66%)</b>	<b>48 (66%)</b>	<b>48 (66%)</b>
	<b>8-cell</b>				<b>-</b>	<b>-</b>	<b>-</b>	<b>-</b>
	<b>16-cell</b>					<b>-</b>	<b>-</b>	<b>-</b>
	<b>Morula</b>						<b>-</b>	<b>-</b>
	<b>Blastocyst</b>						<b>-</b>	<b>-</b>

**Table2 : BrUTP signal in control and CX-5461 treated 2-cell embryos at different time-points on Day 2.** This experiment was performed in triplicate. In the same column, values with different superscripts (a,b) indicate significantly different values ( $p < 0.05$ ; Kruskal & Wallis test)

	N° of embryos	Large BrUTP patches n (%)	Small BrUTP patches n (%)	No BrUTP signal n (%)
Control (D2 +24H)	39	29 (74%) <sup>a</sup>	7 (18%) <sup>a</sup>	3 (7%) <sup>a</sup>
CX-5461 (D2 +24H)	21	5 (24%) <sup>b</sup>	2 (9%) <sup>a</sup>	14 (66%) <sup>b</sup>
CX-5461 (D2 +28H)	39	8 (20%) <sup>b</sup>	15 (38%) <sup>b</sup>	16 (41%) <sup>b</sup>

**FIGURE 1**

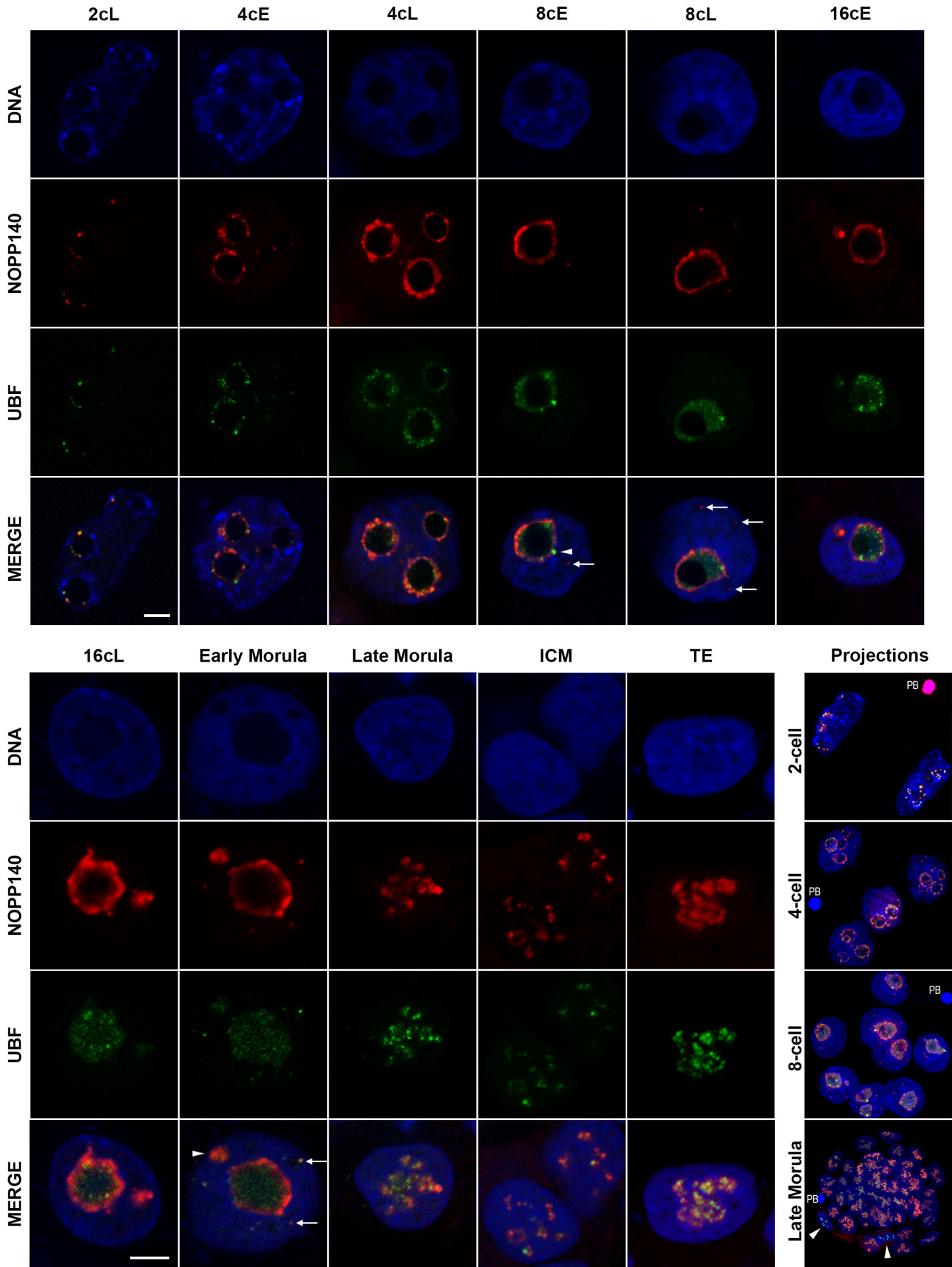


Figure 2

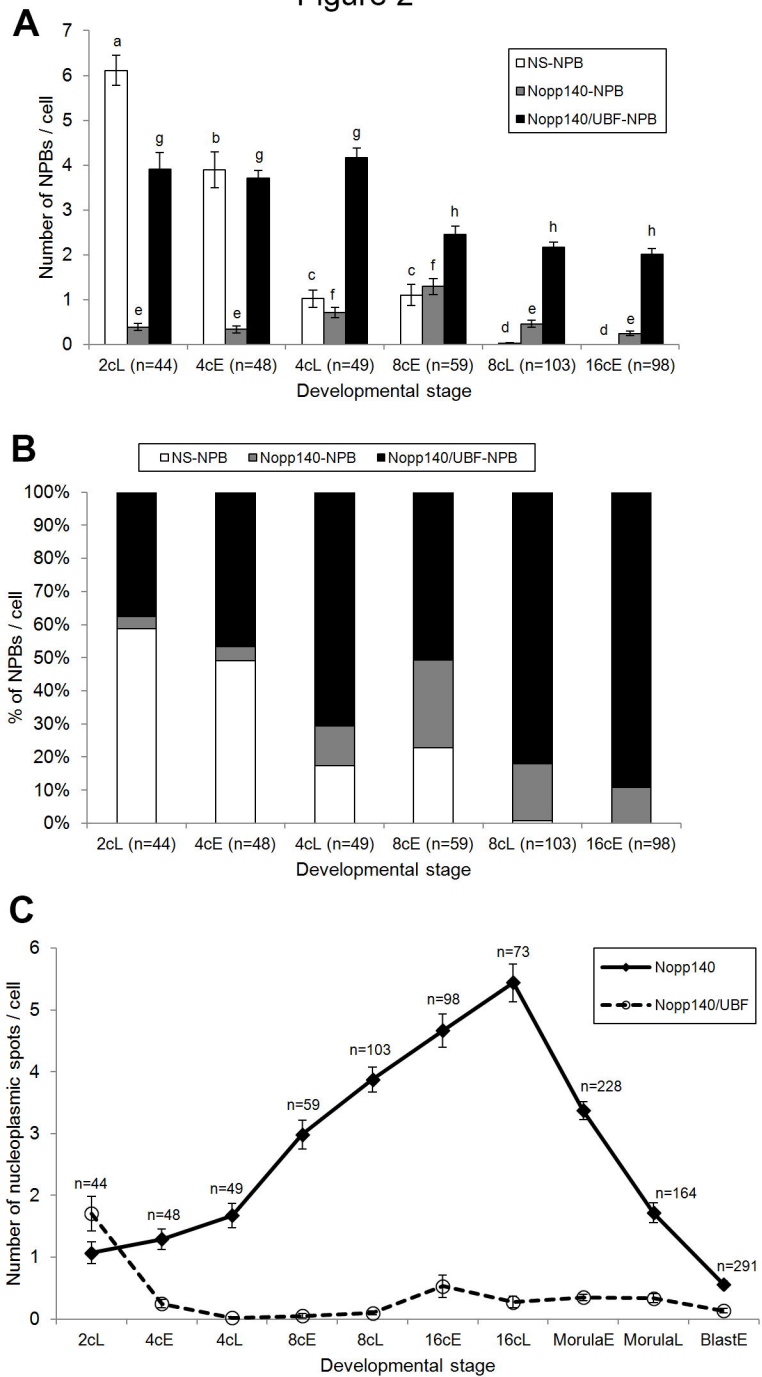
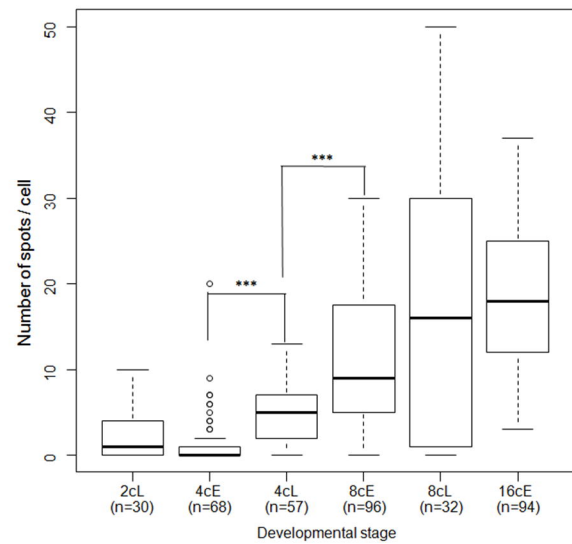
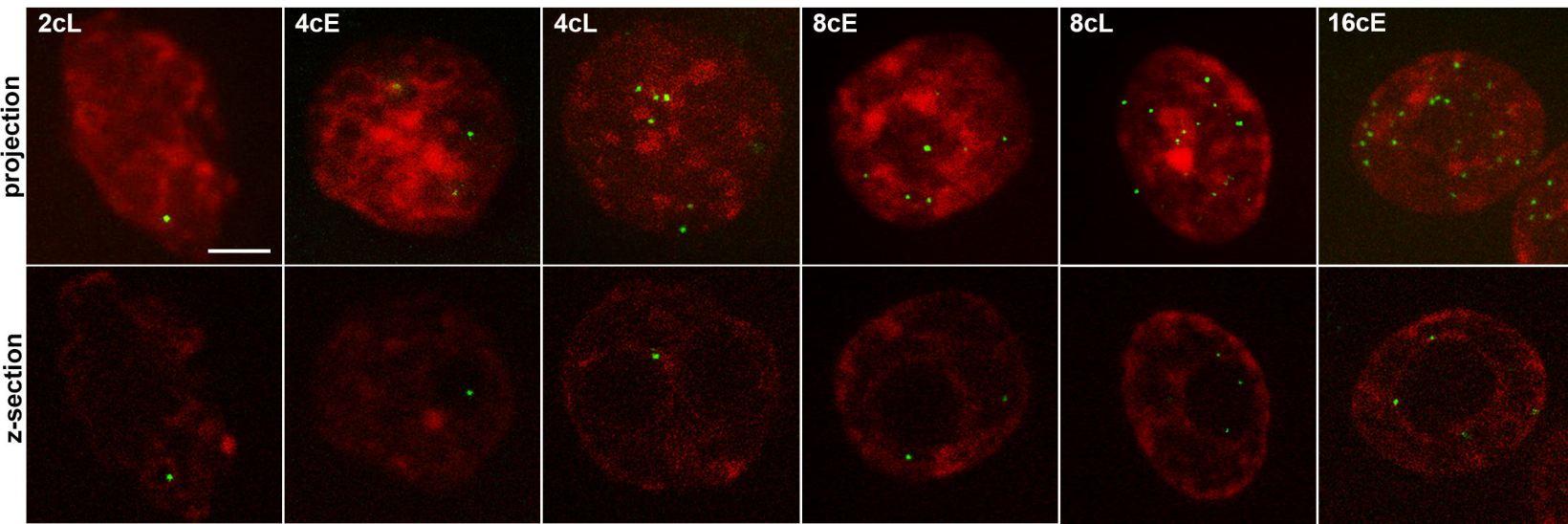


Figure 3



# Figure 4

Control

CX-5461 treatment

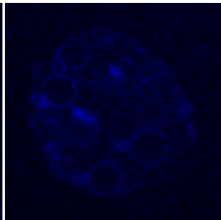
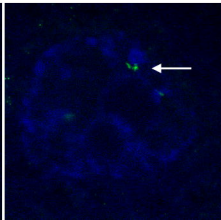
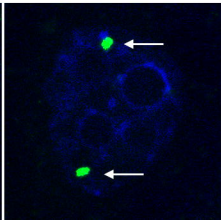
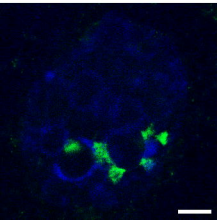




Figure 5

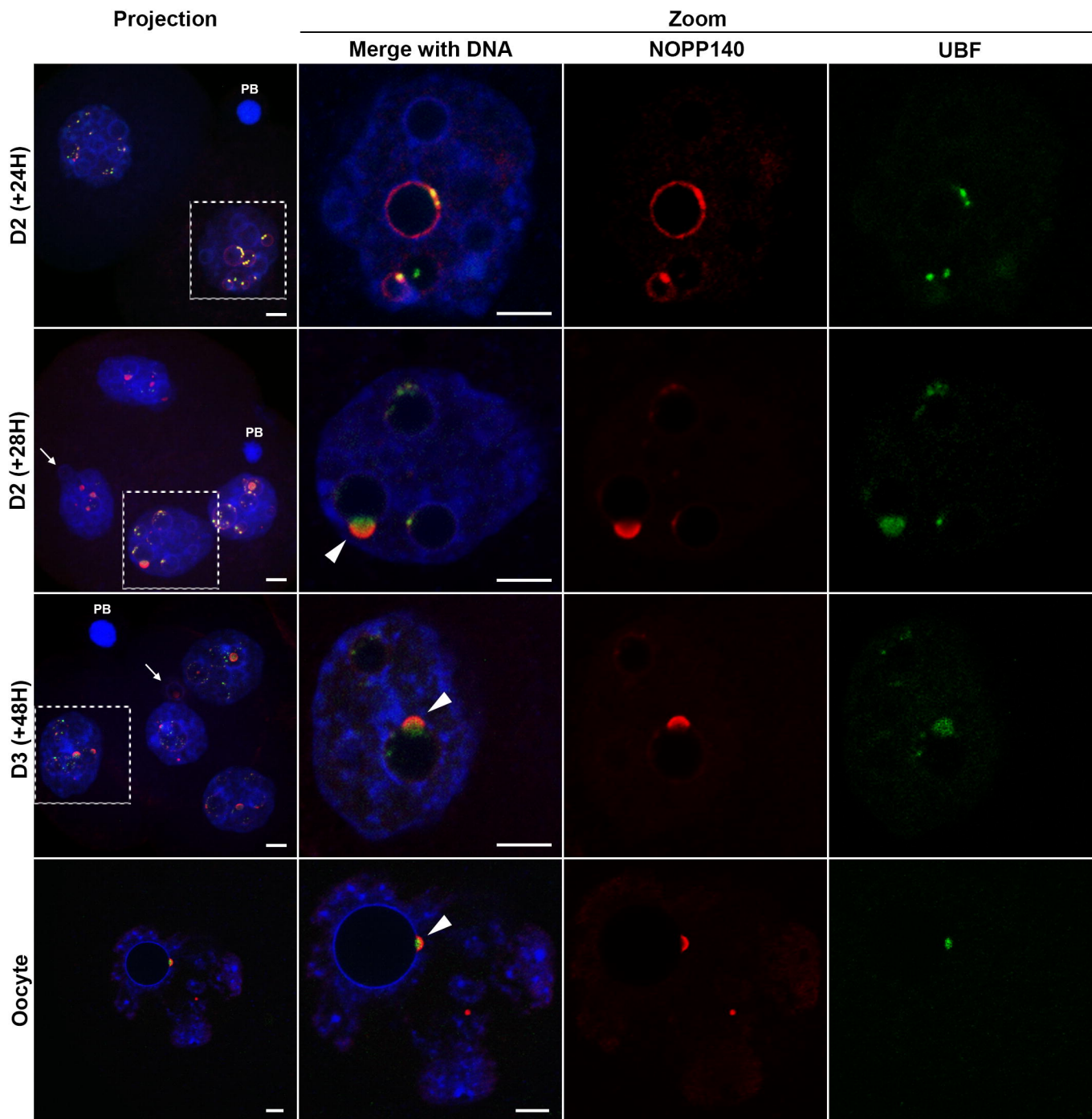


Figure 6

4-cell

